

Comparative modelling of performance limits of solid-state neutron detectors based on planar B-rich capture layers

A D Harken and B W Robertson

Department of Mechanical Engineering and Nebraska Center for Materials and Nanoscience, University of Nebraska-Lincoln, Lincoln, NE 68588-0656, USA

E-mail: brobertson@unl.edu

Received 17 August 2006, in final form 18 August 2006

Published 17 November 2006

Online at stacks.iop.org/JPhysD/39/4961

Abstract

Solid-state neutron detectors based only on boron-rich semiconductors are of interest for their potential to provide the highest thermal neutron detection efficiencies of any solid-state neutron detectors. A simple physical model, recently shown to generate thermal neutron capture product spectra that agree quantitatively with full-physics GEANT4 simulation, is used to compare the capture product energy spectra and the upper limits to neutron detection efficiency of planar conversion layer, sandwich and all-boron-carbide detectors for the case of normally incident, mono-energetic, thermal neutrons. All-boron-carbide semiconductor detectors are deduced to be greatly superior to all other boron-rich solid-state detector types in their maximal neutron detection efficiencies and potential for avoiding false-positive detector output signals in mixed radiation fields. If boron-carbide semiconductors of optimal quality and thickness in the range 20–50 μm were used in creating such detectors, the normal-incidence thermal neutron detection efficiencies could reach 60% to 90%, respectively, in total and still 48% to 78% using only the peak corresponding to the kinetic energy sum for the nuclei emitted in the most-probable $^{10}\text{B}(n,\alpha)^7\text{Li}$ capture reaction.

1. Introduction

Reliable detectors with efficiencies close to 100% for individual neutrons are highly desirable for neutrons with low, thermal (~ 25 meV) and higher kinetic energies. Such detectors are essential for the most challenging applications. These applications include reflectometers and small angle scattering instruments at the next-generation Japanese, American and European spallation neutron sources and, with suitable moderation of neutron energies, monitors for water, gas and oil close to the drill bit during the drilling of holes for geo-exploration, detectors for exploration in space, environmental monitors and monitors for the storage and transport of fissile materials. Many of these applications require detectors to be light, thin, tolerant of extremes of temperature and vibration, low in power demand and insensitive to radiation other than neutrons. For certain spallation source applications, detectors additionally must be

configured as arrays (of area ~ 0.1 – 10m^2) of pixels with size down to $1\text{mm} \times 1\text{mm}$ or less, which are capable of detecting neutrons at rates that may exceed 10^4 neutrons per pixel per second [1].

Gas-filled neutron detectors and scintillator-based neutron detectors are widely used in real-time detection of neutrons of thermal and higher energies [2] but each of these types of detectors has at least one significant drawback that limits its current or potential applications in the areas mentioned above. Solid-state detectors, however, have the potential to overcome most, or all, such limitations simultaneously, but no all-solid-state detector has yet been reported to have neutron detection efficiency close to 100%.

Since neutrons are uncharged, in an ideal real-time solid-state neutron detector, the output signal would be derived from the charge generated during deposition of the full energy of the neutron capture products, including the energy deposited

in the neutron capture region of the detector. This requires the capture region to be semiconducting, in order that all the charge generated by the products of each neutron capture is available to be collected, unlike the case of detectors based on conversion materials that rely on the detection of only those capture products that escape from the capture region. ‘Conversion detectors’ are necessarily restricted in their ultimate performance because capture products lose energy in the capture layer before reaching the adjacent charged particle detector and some capture products never escape from the capture layer. These effects degrade the detectable capture product energy spectra and substantially limit the overall neutron detection efficiency of neutron detectors based on conversion materials. Ideal solid-state detectors would rely on using the neutron capture material as the semiconductor region that primarily detects the neutron capture products; in practice, the performance will be limited by the properties of that semiconductor.

In this paper, we present calculated efficiencies and capture energy spectra obtained by modelling two classes of thermal neutron detectors based on a planar layer of B₅C boron carbide: (1) detectors that only incorporate semiconducting B₅C (all-B₅C detector) and (2) conversion detectors in which a layer of B₅C emits capture products that are only detectable in a charge particle detector on one side (or both sides) of the B₅C layer. We do this for various thicknesses of B₅C layer in order to compare and contrast the detector characteristics, including the upper limits of thermal neutron detection efficiency and the corresponding capture product energy spectra. To simplify the calculations, in common with other authors, we consider neutrons incident with one thermal energy—0.025 eV—and one direction—normal to the capture layer. The results however apply unchanged to other pairs of neutron energy and direction of incidence, as identified in section 4. The reasons for choosing B₅C are presented in section 2; any alternative boron-rich semiconductors which may be shown to serve as semiconducting capture materials in neutron detectors could of course be modelled similarly to later sections of this paper.

2. Semiconducting boron carbide

Boron has a unique combination of characteristics that make it ideal for the formation of a solid-state thermal neutron detector. Boron is one of very few elements that have a large cross section for the capture of thermal neutrons and yield high energy capture product nuclei; for the boron isotope ¹⁰B, which has a natural relative abundance of about 19%, the capture cross section is 3840 b for a 0.025 eV neutron and the capture reaction ¹⁰B(n,α)⁷Li yields 1.47 (1.78) MeV ⁴He and 0.84 (1.02) MeV ⁷Li with 94% (6%) probability—kinetic energies that total 2.31 MeV in the case where a 0.48 MeV γ-ray is emitted and 2.80 MeV otherwise [2]. Boron is unique amongst those elements forming the major component of a refractory ceramic that can also be made as a semiconductor [3, 4]. Therefore, detectors based on boron-rich semiconductors have the potential to be nearly ideal neutron detectors if configured such that ¹⁰B atoms are present in sufficient number density in regions of semiconductor from, or in, which all the capture product ions generate electrical signals that are detected. Such detectors could potentially satisfy all the needs that were identified above.

The problem of creating boron-rich semiconducting boron carbide was solved in the early 1990s [3] and was followed by the creation of a wide range of hetero- and homo-junction diodes and transistors using semiconducting boron carbide, including a heterojunction diode that operates at least at 350 °C [4] and a boron carbide semiconductor/n-Si heterojunction diode neutron detector [5, 6]. Other papers on semiconducting boron carbide materials and devices are also cited in [6]; the semiconducting form of boron carbide in this body of work has compositions close to B₅C. More recently, devices in which the only semiconductor is boron carbide, of either n- or p-type, have been fabricated at the University of Nebraska and confirmed to detect neutrons [7–9].

3. Neutron detection efficiency and capture spectrum

We have adopted a highly simplified calculation, discussed in section 4, to enable us to make a detailed assessment of the spectral and efficiency trends for planar neutron detectors of two types—‘all-B₅C detectors’ that incorporate boron carbide as the only semiconductor and ‘conversion detectors’ that rely on detection of only the capture product(s) that escape(s) from one side, or both sides, of a capture material. This calculation of potentially detectable energy spectra is based on a model similar to the one presented in part by Rossi and Staub [10] for a conversion foil layer in a parallel plate ionization chamber. Approximating the path of an alpha particle in the foil and surrounding gas as a straight one, Rossi and Staub calculated efficiencies for differing thicknesses of the conversion foils, but did not however address the stopping of the 4 different capture product ions. In [10], there is also no discussion of possible output spectra and it is unfortunate that significant portions relating to deposited capture product energy spectra calculations are clearly missing. More recently, Bell *et al* [11] gave equations for planar conversion layers and discussed efficiency as a function of layer thickness, although they also did not present the overall energy spectra of a device based on their model. Using essentially the same model, McGregor and Shultis [12] reported capture energy spectra calculated for all-boron carbide solid-state devices as well as conversion layer devices. However, this work neither provides a comparison of the efficiency of the two types of detector nor discusses the possible attributes of the spectra of an all-boron carbide solid-state device in comparison with those of a conversion layer device, either in the single-sided geometry or in the double-inward, or sandwich, geometry of device. On the basis of their calculations, McGregor *et al* [13] identified the sandwich device as the most efficient topology of solid-state neutron detector; the calculated results we present in this paper lead to quite different conclusions.

Throughout this paper, we have employed the highly simplified linear energy deposition approach on the basis of its suitability to the task because of the close qualitative and quantitative similarity of capture product spectra for conversion B₅C layer, and all-B₅C layer, detection geometries obtained using this simplified approach with the spectra obtained using GEANT4, a full-physics Monte Carlo package. The reader is referred to [14] for this comparison in the case of B₅C layers up to 1 μm thick with natural abundance of

¹⁰B. Such thin layers of B₅C provide a sensitive test of the applicability of the simplified model since, in contrast to the situation for captures occurring deep within the B₅C layer at distances greater than a capture ion range from the layer surface, small deviations from straight paths would take a greater fraction of capture product ions completely out of a thin B₅C layer and variations in ion stopping power along an ion path would affect the energy deposited in a thin B₅C layer by an ion escaping from the layer in one of a wide range of directions.

We conclude therefore that the simplified physical model provides a useful tool that captures even the quantitative trends obtained with a full-physics simulation for capture layers of all thicknesses. Of course, the full-physics approach is highly suited to more complex geometries, such as pixelated detectors, for which the simplified approach would be much less useful.

In section 4, we present our simulation approach in sufficient detail to support the calculated capture energy spectra and integrated efficiency results that we show for both conversion and all-B₅C solid-state thermal neutron detectors. In section 5, we make direct comparison of the spectral characteristics and neutron detection efficiencies of single-sided and double-inward sandwich conversion detectors with those of all-B₅C detectors. Finally, in section 6, we draw conclusions which are relevant to the development of optimally efficient all-B₅C solid-state neutron detectors and their ultimate performance in relation to conversion layer detectors.

4. Simplified physical model for thermal neutron capture detectors

We simulated the potentially detectable capture product energy spectra results given in sections 4–6 on the basis of continuous slowing down of ions travelling along straight paths since, to a first approximation, a light ion loses energy at a constant rate along its path in a material and the paths of energetic light ions are relatively straight until their energies become quite low.

The model relies on these approximations.

1. A neutron entering the layer follows a straight path in the layer.
2. All 0.48 MeV capture gamma rays are ignored.
3. Within the B-containing layer, the variation in stopping power with capture product energy is ignored.
4. Capture products follow straight paths until they stop or escape from the ¹⁰B containing layer.
5. Capture products start in exactly opposite directions.
6. Capture products are emitted in the ratio, and with the energies, appropriate for thermal or cold neutron capture, and the capture cross section is taken to be 3840 b [2].
7. Capture products that leave the layer do not return to the layer.
8. The capture layer is parallel-sided and infinitely wide compared with its thickness.
9. The capture layer is assumed to have a homogeneous neutron capture layer of suitably semiconducting boron carbide of composition B₅C, fully enriched in ¹⁰B, not B₄C, as is the typical description of the material phase known as boron carbide which is not semiconducting.

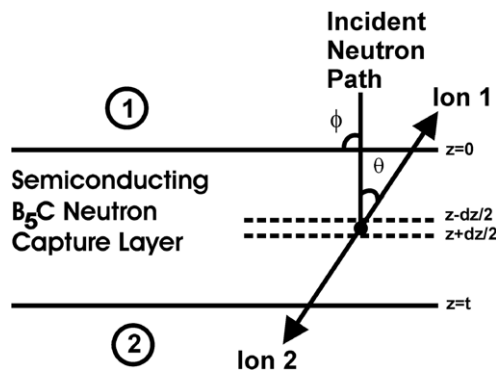


Figure 1. Notation and geometry of semiconducting boron carbide neutron capture layer and capture products, labelled as ions 1 and 2. A conversion detector would involve detection of escaping ions only in regions 1 and/or 2.

We start by considering the case of a capture at a depth z into the layer that results in capture reaction product ions travelling in opposite directions at an angle θ with respect to the normal to the capture layer (figure 1). The energy lost by an ion during its escape from depth z in a direction θ is

$$E_L = \frac{Sz}{\cos \theta}, \quad (1)$$

where the stopping power of the ion in the layer is $S = E/R$, with E and R being the initial energy and the total range of this capture ion in the layer. Because E and R differ for each of the capture products, calculation for each pair of z and θ must be performed individually for each capture product ion. E_L cannot exceed the initial energy of the ion, E_{ion} , and so combinations of z and θ that would provide $E_L > E_{\text{ion}}$ in equation (1) merely define the conditions for capture ions that do not escape from the capture layer because they have lost energy equal to E_{ion} before reaching the surface of the layer. The calculation for the companion ion proceeds in the same manner but with differing E , R and S and with the capture depth, z , replaced by the remaining film thickness $(t - z)$, beyond the capture depth.

Capture of thermal neutrons results in the capture product ions being emitted with equal probability in any direction from the capture location. Therefore, the fraction, $d\eta$, emitted in the range $\theta - \theta + d\theta$ is equal to the fraction $d\Omega/4\pi$ of all solid angles and can be represented as

$$d\eta = \frac{d\Omega}{4\pi} = \frac{2\pi \sin \theta d\theta}{4\pi} = -\frac{1}{2}d(\cos \theta). \quad (2)$$

Equations (1) and (2) provide the basis for analytical calculation of complete energy spectra for each capture product ion. Where analytical results could readily be calculated, these are given in the cases that follow. Where that was not possible, the probability of an incident neutron yielding an ion energy outcome in each capture spectrum energy channel was calculated for successive capture depths at many capture product emission angles and the results were appropriately summed. The calculated probabilities were assigned to energy channel bins 10 keV wide. It was found that steps $dz = 1$ nm and $d(\cos \theta) = 0.0005$ allowed such spectra to be calculated with minimal artefacts. This approach allowed

sufficiently rapid calculation (using Mathcad [15]) such that it was unnecessary to employ a Monte Carlo method of randomized sampling of z and angle.

In each energy channel, the calculated energy spectra we present in this paper provide the probability that capture product ions deposit energy in the range of that channel for each neutron incident on the layer, and so, in the case of ideal detection of the escaping or deposited energies, the spectra yield overall neutron detection efficiencies for each detector type simply by summing the appropriate spectral channels.

These calculated spectra do not incorporate a number of effects that cause the detected spectra and efficiencies to be different in practice. These effects, some of which can be quite significant, include: incomplete sweep-out of charge from the capture product detector to form a charge pulse, mismatch of the pulse processing time and the time profile of this charge pulse and, in the conversion layer case, the additional energy loss from, or the stopping of, the escaping capture products in any intervening material, such as an electrical contact, before they reach the active region of the capture product ion detector. However, as noted in section 1, our goal is to assess the ultimate potential of conversion and all-B₅C semiconductor neutron detectors based on a planar layer of B₅C and to provide a guide to the geometrical and technological requirements of such detectors, and so we do not include these other effects.

4.1. Application to conversion layer detectors

For the case of a conversion layer in which only one ion of each capture product pair is considered at a time, equations (1) and (2) can be combined and then integrated over the full layer thickness, taking the probability of capture per unit depth, n , into account. This results in expressions for the differential probability, dN/dE_L , such that one incident neutron results in an ion that loses energy in the range E_L to $E_L + dE_L$ before escaping from the capture layer; for small t , these expressions are

$$\frac{dN}{dE_L} = \begin{cases} \frac{nSt^2}{4E_L^2} & \text{for } E_L > St \\ \frac{n}{4S} & \text{for } E_L \leq St. \end{cases} \quad (3)$$

The first case in (3) is appropriate for ions with tracks longer than the capture layer thickness and the second case is for ions with tracks shorter than the capture layer thickness.

An ideal conversion layer detector has a 100% efficient particle detector to capture ions that are able to escape from the capture layer. Figure 2 shows the spectrum of energy outcome probabilities for a neutron normally incident on a conversion layer device with an ideal charged particle detector beyond the back of the capture layer surface, i.e. opposite to the neutron entrance surface. Here, exponential attenuation of the neutron flux has been incorporated for all spectra, in contrast to equation (3). There is consequently a maximum spectral integral for a capture layer thickness corresponding essentially to the range of the 1.48 MeV α -particle.

A device with an ideal charged particle detector instead of adjacent to the front, neutron entrance, face (in region 1 of figure 1) would have spectral output similar to figure 2 for layers less than 4.25 μm thick—the range of the higher

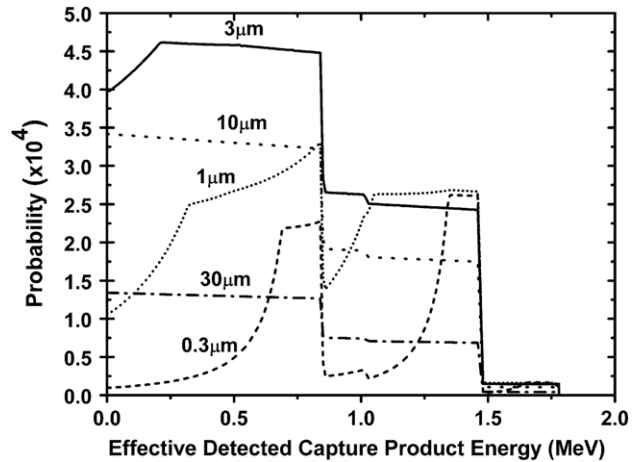


Figure 2. Spectra giving the probabilities, per 10 keV range of deposited capture product energy, that a normally incident neutron will cause capture product energy deposition in a capture product detector beyond the back of the capture layer. The respective capture layer thickness is noted beside each spectrum.

energy α -particle—while spectra from all thicknesses above 4.25 μm would have the shape of the 10 and 30 μm cases, but all would lie atop each other near the level of the 3 μm case because neutron flux attenuation with depth does not affect the entering flux.

Integration of equation (3) over all energies provides the neutron detection efficiencies of ideal devices. For t much smaller than the neutron capture attenuation length (also called the macroscopic absorption capture cross section), the total probability that one incident neutron will result in an ion of one type escaping from the film through either capture layer face is essentially

$$N = \frac{nt}{4} \left(2 - \frac{t}{R} \right) \quad \text{for } t < R, \quad (4)$$

and so

$$N = \frac{nt}{2} \quad \text{for } t \ll R, \quad (5)$$

confirming, of course, that the neutron conversion detector efficiency for an ideal detector with a very thin capture layer will be essentially proportional to layer thickness. (Equations (4) and (5) are also given in [11, 13].)

For layers of thickness t at least equal to ion range R , but still thin compared with the neutron capture attenuation length, the probability that an incident neutron will result in one type of capture product ion that can escape, after losing energy E_L , through a layer face is given by

$$N = \frac{n(E_L)}{4S} \quad \text{for } t \geq R. \quad (6)$$

A standard conversion layer device usually requires an electrical contact layer between the neutron capture layer and the active detection region of the diode that serves as a particle detector. This contact layer results in loss of detectable capture product energy. The extra energy lost in this contact results in an increased total energy loss, E_D , before a capture product ion can reach the particle detector:

$$E_D = E_L + \frac{Scd}{\cos \theta}. \quad (7)$$

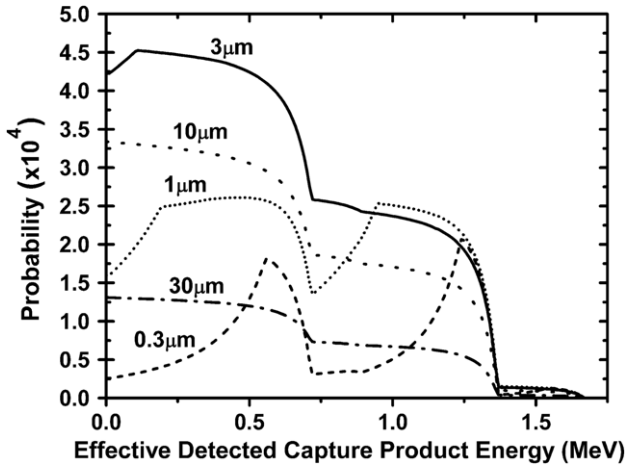


Figure 3. Spectra giving the probabilities, per 10 keV range of deposited capture product energy, that a normally incident neutron will cause capture product energy deposition in a capture product detector separated from the capture layer by a 60 nm Au electrical contact layer. As in figure 2, the ideal particle detector is sited beyond the back of the capture layer and the respective capture layer thickness is noted beside each spectrum.

Here S_C is the stopping power of the contact material, d is the thickness of the contact layer and θ is the starting angle of the capture ion with respect to the contact layer normal. Again, results calculated from equation (7) that yield E_D greater than the initial energy of the ion, E_{ion} , correspond to cases of the ion depositing all energy before being able to escape into the particle detector. To illustrate the effect of a contact on the calculated conversion detector spectrum, a contact layer thickness of 60 nm of gold (as was employed in [13]) was used and the back face detector results, shown in figure 3, used E_D in place of E_L in otherwise similar calculations to those for figure 2.

If the ideal charged particle detector was instead adjacent to the neutron entrance (front) face, all the energy spectra for thicknesses greater than $4.25 \mu\text{m}$ would again lie atop one another close to the $3 \mu\text{m}$ spectrum.

The sandwich, or double-inward, detector [13, 16] employs charged particle detectors adjacent to both front and back surfaces of the neutron capture layer (in both regions 1 and 2 of figure 1). If the capture layer is thin enough, this device geometry makes possible the detection of both ions from a neutron capture product pair, allowing for detection of more of the capture product energy if the particle detector outputs are summed to account for coincident ion pairs. The energy that could be detected in this case is

$$E_T = E_{\text{sum}} - E_{L1} - E_{L2}, \quad (8)$$

where E_{sum} is the total initial energy of the capture product ion pair and E_{L1} and E_{L2} refer to the energies lost by the ions before they escape from opposing surfaces of the capture layer. Note that, in the cases of only one ion escaping from the capture layer or neither ion escaping from the capture layer, the escaping ion energy, and so neutron detectability, is just the same as for the single-sided detector case.

The double-inward sandwich detector spectra, calculated without contact layers on either capture layer surface, are given

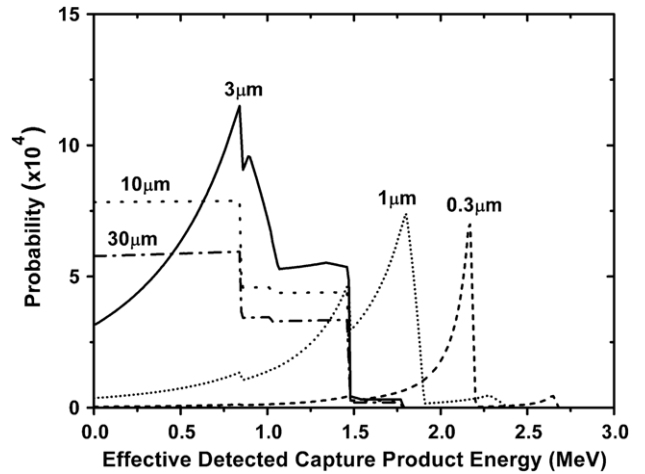


Figure 4. Spectra giving the probabilities, per 10 keV range of deposited capture product energy, that a normally incident neutron will cause capture product energy deposition in ideal capture product detectors which sandwich the neutron capture layer and whose outputs are summed in coincidence. The respective capture layer thickness is noted beside each spectrum.

in figure 4 for the same capture layer thicknesses as in figures 2 and 3. For capture layers much thinner than the range of the Li capture ions, there are peaks corresponding to detection of both capture products for both the γ -emission and non- γ results of neutron capture by ^{10}B . The peak corresponding to the major branching ratio result ($E_{\text{sum}} = 2.31 \text{ MeV}$) occurs at a lower energy than 2.31 MeV because of the energy lost in the capture material.

If this peak alone were used in order to try to create a detection system that discriminated against detection of radiation that resulted in outcomes equivalent to other energies, the effective neutron detection efficiency reaches higher probabilities of an incident neutron giving an outcome in some spectral channels than in the single-sided conversion layer case. It is notable that the detection efficiency in all cases would be under 2%, a result obtainable by integrating the spectral content of this peak. When the capture layer thickness is increased to little more than $1 \mu\text{m}$, this peak merges with the rest of the capture product energy range of the single-side conversion detector spectra making discrimination difficult if not impossible. However, because of the sandwich detection symmetry and neutron absorption, it is apparent from comparison of figures 2 and 4 that the neutron detection efficiency of a sandwich detector with a single capture layer at best only approaches twice that of the single-sided conversion layer detector.

4.2. Application to all- B_5C detectors

Although the energy deposited in the capture layer by each individual ion is simply evaluated for each capture depth z within the layer and for each capture ion starting angle, the calculation of the all- B_5C detector spectra requires numerical evaluation because of the differing stopping powers of the individual ions, just as in the case of the double-inward sandwich with the thinner capture layers. In this case, the total energy deposited in the layer by a capture ion product

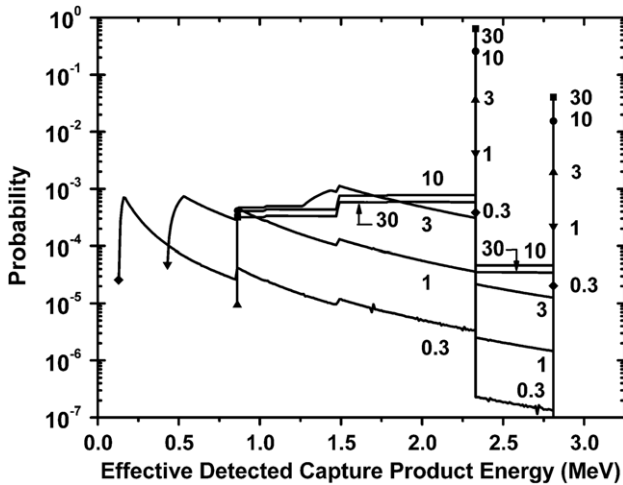


Figure 5. Spectra giving the probabilities, per 10 keV range of deposited capture product energy, that a normally incident neutron will cause capture product energy deposition in a ^{10}B enriched all- B_5C detector. The respective capture layer thicknesses in μm ($0.3\ \mu\text{m}$ (\blacklozenge), $1\ \mu\text{m}$ (\blacktriangledown), $3\ \mu\text{m}$ (\blacktriangle), $10\ \mu\text{m}$ (\bullet) and $30\ \mu\text{m}$ (\blacksquare)) thick are noted beside each spectrum both numerically and symbolically to avoid confusion.

pair becomes

$$E_T = E_{\text{sum}} - (E_1 - E_{L1}) - (E_2 - E_{L2}). \quad (9)$$

Here E_T is the energy at which the correct dN/dE_L fraction, calculated previously for the given E_L of the ion, is contributed to the pulse height spectrum, shown in figure 5 for a range of capture layer thicknesses. In equation (9), $E_1 - E_{L1}$ and $E_2 - E_{L2}$ are the remaining energies for the two ions of the capture pair. As the capture layer thickness increases, $E_1 - E_{L1}$ and $E_2 - E_{L2}$ will on average tend towards zero as many of the neutron captures will occur, of course, deep enough within the layer such that neither ion will be able to escape from the layer. In this case, there is 100% detectability of the capture products and these products contribute full energy deposition in the ion detection layer (the capture layer):

$$E_T = E_{\text{sum}}. \quad (10)$$

We note that, extending the simplified physical model calculations to thicker B_5C layers, there are significant changes between the spectra in figure 5. In contrast to figures 2–4, the probability of an incident neutron giving a capture product output in each energy channel is plotted logarithmically in figure 5; this is necessary because the probabilities in both all- B_5C detector full-energy peaks (corresponding to both the γ -emission and non- γ results of neutron capture by ^{10}B) are so high once the capture layer thickness exceeds a micrometre or two.

The full-energy peaks corresponding to both the γ -emission and non- γ results of neutron capture by ^{10}B become by far the most prominent features for capture thicknesses significantly greater than $1\ \mu\text{m}$. At capture layer thicknesses of $3\ \mu\text{m}$ and greater, the $2.31\ \text{MeV}$ full-energy peak alone provides a probability of neutron detection equal to, or exceeding, that of any B_5C conversion layer detector.

For thicknesses such as $3\ \mu\text{m}$ that exceed the range of the ^7Li capture products, the minimum energy deposited is equal to the full energy of the ^7Li capture products. For this, and greater, thicknesses the steps observed in spectra correspond to successive additions to the energy deposition at energies exceeding the energy of each capture product. For a $3\ \mu\text{m}$ thick layer, there is a remnant of the spectral energy shape found at lower thicknesses since the ranges of both energies of ^4He capture product still exceed the layer thickness.

5. Comparison of conversion and all- B_5C spectra

Figure 6 provides a direct comparison of the conversion layer, sandwich and all- B_5C detector capture energy spectra for a $3\ \mu\text{m}$ thick B_5C layer. Even at this thickness, the full-energy peaks corresponding to deposition of all the energy of both capture products are an important aspect of all- B_5C spectra. The total neutron detection efficiencies are given by the integrals of these spectra. Thus, even with a B_5C layer only $3\ \mu\text{m}$ thick, the potential neutron detection efficiency of an all- B_5C device is much greater than that of the single-side conversion layer device or the sandwich device.

Both the sandwich and the single-sided conversion layer devices lose in efficiency because capture product ions fail to reach the ion detection region. This loss of detectability cannot occur in the all- B_5C device since capture ion detection occurs in the capture region.

For several reasons, discussed below, the energy ranges of significant probability in these spectra are highly relevant to neutron detection with real pulse processing electronics and with the necessary electrical contacts.

The effect of energy lost by capture products in a $60\ \text{nm}$ Au electrical contact between a conversion layer and its associated capture product detector was shown in figure 3, but is seen more clearly by comparing the conversion layer cases in figure 6. The neutron capture spectra of both the sandwich and single-sided conversion layer cases have significant content in the low-energy range where there will, in practice, be additional contributions to the spectrum due to electrical noise from the capture product detection system. This detection system noise will further limit the device efficiency by requiring the use of a threshold, for example at $300\ \text{keV}$, to avoid false counts, thereby eliminating detection of capture energy outcomes in the range below the threshold energy. For sandwich devices with B_5C films up to $1\ \mu\text{m}$ thick, there is evidence of peaking near the original full energy of the emitted capture ion products. However, as noted earlier, the resulting peaks in these cases correspond to integrated detection efficiencies of less than 2%. The sandwich device also presents the difficulty that, if the two charged particle detectors are not operated in coincidence, there will be some double counting of capture events in the case of capture layers thinner than the maximum range of the combined ion pairs.

For all- B_5C semiconductor neutron detectors with B_5C layers at least 2 or $3\ \mu\text{m}$ thick, the $0.84\ \text{MeV}$ minimum energy in the spectra due to the full-energy deposition of one Li^7 ion means that there is a large separation of all spectral features from any energies equivalent to electrical or other noise in the detection system. Unlike the conversion layer case, the minimum spectrum energy is significantly above the energies

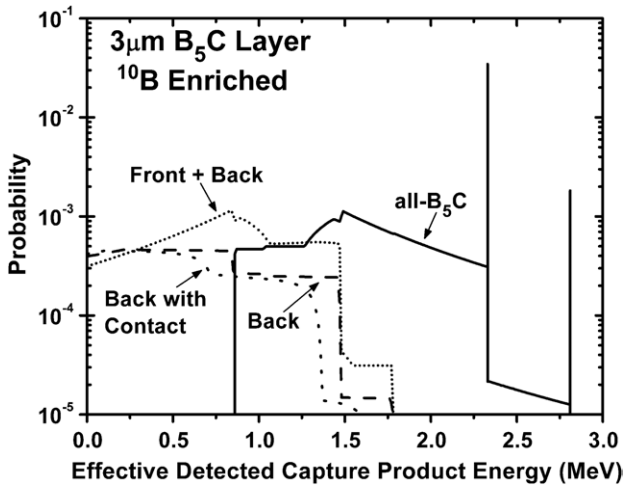


Figure 6. Spectra giving the probabilities, per 10 keV range of deposited capture product energy, that a normally incident neutron will cause capture product energy deposition in an ideal conversion layer ion detector, a conversion layer ion detector with an 60 nm Au contact layer, an ideal sandwich conversion layer ion detector and an ideal all-B₅C detector based in each case on a 3 μm thick B₅C layer fully enriched in ¹⁰B.

associated with any detection system noise and, further, most of the spectral content is well above this minimum energy. Therefore, even with quite severe signal degradation in the detection system, there would be no significant losses in neutron detection efficiency, whether or not a lower capture product detection energy threshold was applied. Electrical contacts adjacent to an all-B₅C detector only serve to apply voltage to the detector and to sweep out the electron-hole pairs created in the layer by pairs of capture products, but do not degrade the spectra or reduce the neutron detection efficiency.

Of course, the all-B₅C spectral features will be broadened in practice because of electronic noise, charge collection and pulse processing effects. This means that the full-energy peaks will be spread over multiple 10 keV channels, rather than occupying a single channel as presented in figures 5 and 6. Nevertheless, as long as charge collection and processing from the all-B₅C device is reasonably efficient, the major full-energy peak can be expected to contribute a clearly distinguishable feature of the measured capture energy spectrum and therefore to provide an excellent opportunity to implement window energy discrimination to yield a thermal neutron detector that is exceedingly insensitive to radiation detected at different energies.

The integrated efficiencies of the conversion layer, sandwich and all-B₅C detectors are presented in figure 7 as a function of the thickness of the B₅C neutron capture layer. At layer thicknesses above a few micrometres, the efficiency of the all-B₅C detector is significantly above the ideal efficiencies of both the conversion layer devices and the sandwich layer device. At thicknesses about 50 μm, the sandwich layer device efficiency will tend towards the efficiency of a standard conversion layer device due to exponential neutron attenuation in the capture layer. This effect can be seen in figure 2 as an overall spectral height decrease with increase in the film thickness for a standard conversion layer. Included in figure 7

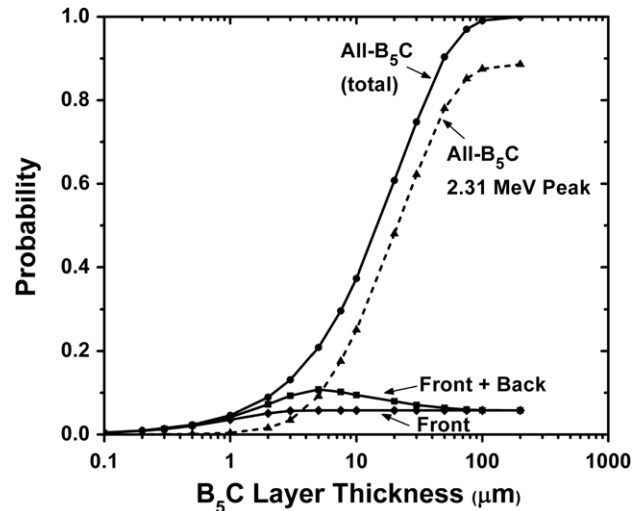


Figure 7. Upper model limits of neutron detection efficiency as a function of ¹⁰B₅C capture layer thickness for sandwich (front + back) conversion layer standard front side conversion layer, and all-B₅C semiconducting neutron detectors. Also shown is the full energy peak (2.31 MeV) for the all-B₅C case. The straight lines between symbols serve only to guide the eye between calculated data points.

are the efficiencies for a conversion layer device with a charged particle detector adjacent only to the neutron entrance (front) face. Also shown for comparison in figure 7 is the probability of a neutron capture event in an all-B₅C detector resulting in the case of full-energy deposition (2.31 MeV) for the major capture branching ratio case. This clearly indicates the potential to use an energy discrimination ‘window’ to select this energy range for highly efficient neutron detection. Thus, using this spectral feature alone would not only nearly eliminate false positives at the cost of only a very slight loss in overall neutron detection efficiency, but, for capture layer thicknesses greater than 6 μm, would still result in greater neutron detection efficiencies than achievable by either the sandwich devices or conversion layer devices.

Throughout this paper we have used a single planar layer for convenience in the modelling. Certainly having capture material in narrow rods, pits or trenches might enhance the detection efficiencies in some circumstances for a conversion layer style device, particularly if neutrons are incident in directions for which the projected thickness of the capture layer is comparable to the macroscopic cross section for neutron capture [17]. A rod, trench or filled-dimple geometry would modify the energy distribution of the capture products somewhat, but the spectral trends of the single-sided and sandwich conversion detectors must still be limited by the energy that is lost before these capture product ions escape into the electrically active regions where they can be detected. With the drawbacks of complexity, ion detection and cost, use of multiple conversion layers could also permit increase in neutron capture and detection efficiency if the capture product ions are appropriately detected. However, the conclusions we have drawn in this paper from the comparison of the conversion and all-B₅C detectors are not expected to change in any significant way because of an increased number of converters or a change in the shape of capture material.

6. Conclusions

In this paper we have used a simplified model to enable comparison of planar all-B₅C-semiconductor thermal neutron detectors and thermal neutron detectors based on a layer of B₅C that acts as a conversion layer from which neutron capture products are only potentially detectable after they escape from the capture material. For all thicknesses of capture layers above about 1 μm, the ideal all-B₅C device would have a detection efficiency advantage over ideal conversion layer devices based on a single planar layer of B₅C. This advantage is nearly a factor of two near a capture thickness of 5 μm and is increasingly more pronounced at all greater thicknesses, with the thermal neutron detection efficiency of an ideal all-B₅C device rising to close to 100%.

To have the potential to attain normal-incidence thermal neutron detection efficiencies of 50%, an ideal ¹⁰B-enriched all-B₅C-semiconductor detector would only need to be 14.5 μm thick; thicknesses greater than 50 μm would potentially provide at least 90% efficiency.

While not becoming a significant part of the full all-¹⁰B₅C device integral until the B₅C device is nearly 2 μm thick, the 2.31 MeV peak alone comprises half the all-B₅C capture spectrum for a capture layer thickness of 5 μm. On its own, this peak would yield a neutron detection efficiency of 62% (88%) for B₅C layers 30 μm (100 μm or more) in thickness. This is accompanied by an absence of capture spectral content at energies below 0.84 MeV and so an absence of the potential for electronic noise, x-rays or many other types of radiation to cause a signal that might be mistaken for a neutron-caused signal. The conversion devices have capture spectra whose energy content is mostly at relatively low equivalent capture product energy, except in the case of sandwich devices with capture layers thinner than about 1.5 μm, for which the energy-shifted version of the 2.31 MeV peak contributes a normal incidence thermal neutron detection efficiency under 2%. For attaining high neutron detection efficiency without ‘false-positive’ signals in mixed radiation fields, such as those in many applications identified in the introduction, the all-B₅C semiconducting detectors therefore have key potential advantages over conversion layer devices because of the dominance of the 2.31 MeV full-energy peak and the absence of low-energy capture spectral content.

As discussed, these conclusions are largely unchanged for any variants of conversion material detectors, including more complex geometries of capture material sandwiched by a capture product ion detector. Whether the potential of all-B₅C-semiconductor devices as neutron detectors can be fully realized depends on being able to sweep out and process the charge resulting from each neutron capture efficiently and quickly enough.

Acknowledgments

The support of the National Science Foundation through Grants #ECS-0300018, the National Aeronautics and Space Administration through Grant NNG05GM89G issued through the Astrobiology, Science and Technology Instrument

Development Program, Office of Naval Research, and the US Department of Energy National Nuclear Security Administration Office of Nonproliferation Research and Engineering (NA-22) through Pacific Northwest National Laboratory is gratefully acknowledged.

References

- [1] Crawford R K and SNS Instrument Systems Team 2002 Neutron scattering instrumentation at the spallation neutron source *Advances in Neutron Scattering Instrumentation* ed I S Anderson and B Guerard *Proc. SPIE* **4785** 10–23
- [2] Knoll G F 2000 *Radiation Detection and Measurement* 3rd edn (New York: Wiley)
- [3] Lee S, Mazurowski J, Ramseyer G and Dowben P A 1992 Characterization of boron carbide thin films fabricated by plasma enhanced chemical vapor deposition from boranes *J. Appl. Phys.* **72** 4925–33
- [4] Adenwalla S, Welsch P, Harken A, Brand J I, Sezer A and Robertson B W 2001 Boron carbide/n-silicon carbide heterojunction diodes *Appl. Phys. Lett.* **79** 4357–9 and references therein
- [5] Robertson B W, Adenwalla S, Harken A, Welsch P, Brand J I, Dowben P A and Claassen J P 2002 A class of boron-rich solid-state neutron detectors *Appl. Phys. Lett.* **80** 3644–6
- [6] Robertson B W, Adenwalla S, Harken A, Welsch P, Brand J I, Claassen J P, Boag N M and Dowben P A 2002 Semiconducting boron-rich neutron detectors *Advances in Neutron Scattering Instrumentation* ed I S Anderson and B Guerard *Proc. SPIE* **4785** 226–33
- [7] Caruso A N, Billa R B, Balaz S, Brand J I and Dowben P A 2004 The heteroisomeric diode *J. Phys. Condens. Matter* **16** L139–46
- [8] Diaz M L, Day E E and Adenwalla S 2006 Neutron detection in all-boron-carbide devices, in preparation
- [9] Caruso A N *et al* 2006 The all boron carbide diode neutron detector: comparison with theory *Mater. Sci. Eng. B* **135** 129–33
- [10] Rossi B B and Staub H H 1949 *Ionization Chambers and Counters: Experimental Techniques* 1st edn (New York: McGraw-Hill)
- [11] Bell Z W, Buckner M A and Smith D B 1996 A ¹⁰B-based solid-state thermal neutron detector *Nucl. Mater. Manag.* **25** 414–9
- [12] McGregor D S and Shultis J K 2004 Spectral identification of thin-film-coated and solid-form semiconductor neutron detectors *Nucl. Instrum. Methods Phys. Res. A* **517** 180–8
- [13] McGregor D S, Hammig M D, Yang Y H, Gersch H K and Klann R T 2003 Design considerations for thin film coated semiconductor thermal neutron detectors I: basics regarding alpha particle emitting neutron reactive films *Nucl. Instrum. Methods Phys. Res. A* **500** 272–308
- [14] Lundstedt C N, Harken A D, Day E E, Robertson B W and Adenwalla S 2006 Modeling solid-state boron carbide low energy neutron detectors *Nucl. Instrum. Methods Phys. Res. A* **562** 380–8
- [15] *Mathcad 2000 User's Guide* (Cambridge, MA: Mathsoft Engineering and Education)
- [16] McGregor D S, Klann R T, Gersch H K, Ariesanti E, Sanders J D and VanDerElzen B 2002 New surface morphology for low stress thin-film-coated thermal neutron detectors *IEEE Trans. Nuc. Sci.* **49** 1999–2004
- [17] Shultis J K and McGregor D S 2006 Efficiencies of coated and perforated semiconductor neutron detectors *IEEE Trans. Nucl. Sci.* **53** 1659–65